

Pressure driven spinning: A multifaceted approach for preparing nanoscaled functionalized fibers, scaffolds, and membranes with advanced materials

Suwan N. Jayasinghe^{1,a)} and Nicolai Suter²

¹*Department of Mechanical Engineering, BioPhysics Group, University College London, Torrington Place, London WC1E 7JE, United Kingdom*

²*Nisco Engineering AG, Dufourstrasse 110, 8008 Zurich, Switzerland*

(Received 1 December 2009; accepted 1 February 2010; published online 2 March 2010)

Electrospinning, a flexible jet-based fiber, scaffold, and membrane fabrication approach, has been elucidated as having significance to the health sciences. Its capabilities have been most impressive as it possesses the ability to spin composite fibers ranging from the nanometer to the micrometer scale. Nonetheless, electrospinning has limitations and hazards, negating its wider exploration, for example, the inability to handle highly conducting suspensions, to its hazardous high voltage. Hence, to date electrospinning has undergone an exhaustive research regime to a point of cliché. Thus, in the work reported herein we unveil a competing technique to electrospinning, which has overcome the above limitations and hazards yet comparable in capabilities. The fiber preparation approach unearthed herein is referred to as “pressure driven spinning (PDS).” The driving mechanism exploited in this fiber spinning process is the pressurized by-pass flow. This mechanism allows the drawing of either micro- or nanosized fibers while processing polymeric suspensions containing a wide range of advanced materials spanning structural, functional, and biological entities. Similar to electrospinning if the collection time of these continuous formed fibers is varied, composite scaffolds and membranes are generated. In keeping with our interests, multicompositional structural entities such as these could have several applications in biology and medicine, for example, ranging from the development of three-dimensional cultures (including disease models) to the development of synthetic tissues and organ structures to advanced approaches for controlled and targeted therapeutics. © 2010 American Institute of Physics.

[doi:[10.1063/1.3328092](https://doi.org/10.1063/1.3328092)]

I. INTRODUCTION

Recent literature has demonstrated electric field driven jetting techniques having significant utility in a wide range of applications within the health sciences.^{1,2} These have resulted with the widespread research and developmental studies that have been carried out with both electrosprays and electrospinning. The techniques largely exploit a conducting needle, held at a voltage generally in the thousands of volts, with respect to a grounded electrode. The media flowing within the needle undergo charging and subsequently enter an external electric field, accelerating the media toward the grounded electrode.³ The detail distinguishing electrospraying from electrospinning is that the former generates droplets, while the latter forms fibers, which on collection over a function of time form scaffolds and membranes. Both these approaches have been extensively demonstrated for generating droplets and fibers in the nanometer scale^{4,5} while handling a wide range of

^{a)}Author to whom correspondence should be addressed. Electronic mail: s.jayasinghe@ucl.ac.uk. Tel.: +44 (0)2076792960. FAX: +44(0)2073880180.

material loaded suspensions with large bore needles ($>500 \mu\text{m}$). This is a unique feature of these techniques, thus superseding its rival, namely, ink-jet printing, known to form droplets and/or fibers approximately double the size of the needle used.⁶

Recent research into these techniques has seen some unique developments. First, electrosprays in conjunction with living sols have demonstrated the forming of three-dimensional structures (with unassisted overhangs) to even fibers and scaffolds.⁷⁻⁹ This achievement results directly with the fine-tuning of living sols while establishing control over the electric field. Although on many previous occasions both electrosprays and electrospinning have generated structures and subsequently been explored in biomedical applications, the techniques were never applied directly to the handling of living entities. In 2005/2006, this was achieved with both these techniques, which are now referred to as “bio-electrosprays” and “cell electrospinning,” demonstrating the ability to handle a wide range of living cells (immortalized, primary to stem cells) to even whole organisms.¹⁰⁻¹⁴

Although, there has been much success with these techniques, they carry with them two significant limitations, namely, the inability to handle highly conducting suspensions while operating in stable and continuous conditions in the single needle configuration (in open-air ambient scenarios) to the hazardous driving mechanism. These obstacles, to some extent, limit the exploration of these approaches demanded for intravenous medical applications, for example, if required for repairing damaged cardiac tissue soon after myocardial infarction. Nonetheless, these limitations have spurred us to investigate and develop a competing technology, completely driven by means of a pressurized by-pass flow.

The technology unveiled herein generates composite solid and hollow fibers to those that contain multistructural morphologies (porous and hollow) at similar dimensions to those reported in electrospray/electrospinning studies. Interestingly none of the limitations faced by both these techniques, namely, (i) the inability to handle highly conducting media/suspensions and (ii) the hazardous operational voltage, are applicable to this pressure driven spinning methodology. We envisage our findings on this multifaceted fiber, scaffold, and membrane fabrication approach to be explored in many fields of research within the health sciences, where such structural architectures have been demonstrated as having widespread applications.

II. EXPERIMENTAL SECTION

A. Pressure driven devices

The devices used in these studies explore stainless steel medium bore needles, which have an inner bore diameter varying from a few to several hundred micrometers. The single needle device was manufactured in polyether ether ketone [Figs. 1(a) and 1(b)], while the coaxial or concentric device [Figs. 1(c) and 1(d)] was fabricated with stainless steel (316L). Both these devices are autoclavable. The chamber volume for the single needle device is $\sim 770 \text{ mm}^2$ (which could be varied along with the connecting screws) and allows the protruding needle at the chamber, extend a few millimeters from the base of the exit orifices. The orifices are $\sim 600 \mu\text{m}$ in diameter and are focused to the protruding needle. In the case of the coaxial or concentric needle device, the needle bore diameters varied from the few hundred to several hundreds of micrometers. The chamber volume is $\sim 4100 \text{ mm}^2$, with the exit orifices focusing to the needles.

B. Materials

In these investigations several polymers were explored, namely, poly(ethylene oxide) [PEO, $M_w = 100\,000$], poly(ϵ -caprolactone) [PCL, $M_w = 80\,000$], polyvinyl alcohol [PVA] (all three purchased from Sigma-Aldrich, Gillingham, United Kingdom), and poly(L-Lactic acid) [PLLA, $M_w = 700\,000$] (purchased from Polysciences, Inc., Warrington, USA). To these polymer solutions, we decided to add nanomaterials, demonstrating future possible exploration of this approach for bearing nanomaterials, for controlled and targeted drug delivery. To this end SiO_2 nanoparticles

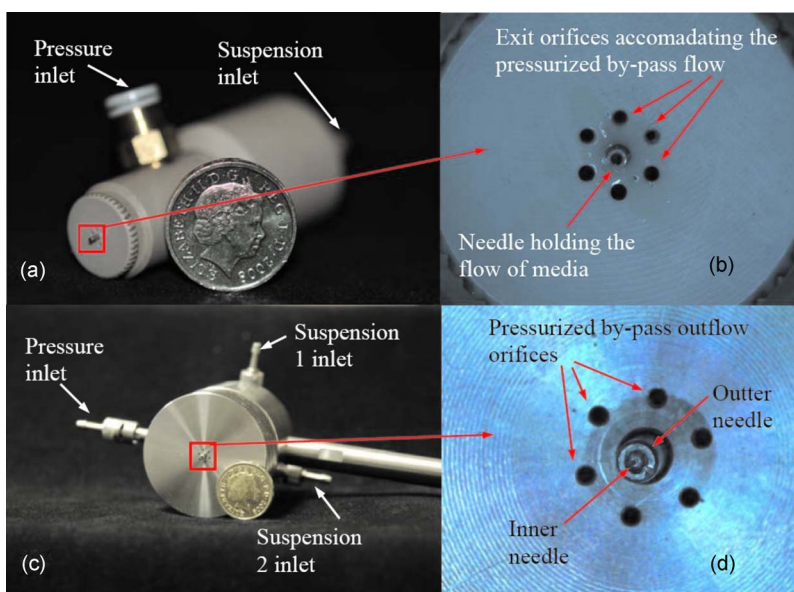


FIG. 1. Representative digital images and optical micrographs of the pressure driven devices explored in these studies. (a) The single needle device and (b) the single needle exit, (c) the coaxial or concentric needle device, and (d) the concentric needle exit.

and the multiwalled carbon nanotubes (bamboo-type) were explored in these studies, which were provided in-kind by Nyacol Nanotechnologies, Inc., and NanoLab, Inc., both companies based in Massachusetts, USA.

C. Polymer and cell suspension preparation

The polymers were dissolved in their respective solvents as previously reported,^{15–18} while magnetic stirring was carried out overnight assuring the formulation of a near-homogeneous free-running solution. In the preparation of nanosuspensions (containing either SiO₂ nanoparticulates or bamboo-type multiwalled nanotubes), the given polymer was first prepared into a free-running solution and later introduced to the nanomaterials at calculated concentrations while magnetically stirred. Sedimentation tests were carried out at a wide range of intervals (1, 3, 5, 7, and 24 h) and found to be negligible. However, in these studies the prepared nanosuspensions were spun within 1 h of preparation. For assessing cell nesting within fibers, cell suspensions were prepared by employing human embryonic kidney cells (HEK 293T) stably expressing enhanced Green Fluorescent Protein (eGFP). Briefly, the cells were transfected with lentivirus with an eGFP construct (SFFV-eGFP-WPRE).^{19,20} The eGFP positive cells were then sorted and propagated *in vitro*. The cells were cultured in Dulbecco's Modified Eagle's Medium (4.5 g/l liquid with sodium pyruvate with l-glutamine, PAA, Laboratories Ltd., Yeovil, United Kingdom) supplemented with 10% fetal bovine serum (gold, heat inactivated, EU approved, PAA, Laboratories Ltd., Yeovil, United Kingdom). To prepare the adherent HEK 293T eGFP-expressing cells for spinning, the cells were washed with Dulbecco's Phosphate Buffered Saline (1X without Ca and Mg, PAA, Laboratories Ltd., Yeovil, United Kingdom) followed by the addition of 0.5% trypsin/ethylenediaminetetraacetic acid (EDTA) (PAA, Laboratories Ltd., Yeovil, United Kingdom) at approximately 2 ml per 75 cm² of the cellular monolayer. The cells were incubated in trypsin/EDTA for 5 min at 37 °C and 5% CO₂. The loosened cells were collected and then pelleted by centrifugation at ~1000g for 5 min (Hettich, Rotofix 32A). The supernatant was removed, and the pellet was resuspended in growth medium. Using a digital hemocytometer (countess automated cell counter, Invitrogen, Paisley, United Kingdom), cell counts were carried out. The formulated ready-to-spin cell suspension was at a cellular concentration of ~10⁶ cells/ml. Similarly, these

cells were prepared for assessing cell viability exploring flow cytometry; however for these viability studies the cells did not have the eGFP construct.

D. Fiber, scaffold, and membrane characterization

The generated structures were characterized using optical/fluorescence Leica Microscopes (Milton Keynes, United Kingdom), models DMIL (inverted) and DM2500, respectively. These microscopes were also employed for the cell phenotypic studies carried out in this work. Generated structural characterization of the fibers, scaffolds, and membranes was mainly carried out using scanning (JOEL JSM 6301F, Herts, United Kingdom) and transmission (model JEOL 1010, Herts, United Kingdom) electron microscopes based in the Chemistry and the Anatomy Departments at University College London. For optical and fluorescence microscopy, structures were collected onto glass microslides, while for scanning electron microscopy (SEM) and transmission electron microscopy (TEM), fibers were collected onto SEM stubs and TEM grids having a mesh density of 100, respectively (purchased from Agar Scientific Ltd, Essex, United Kingdom).

E. High-speed digital image capturing

Throughout these studies spinning behavior was studied by means of a digital high-speed camera in real time (Phantom V7.3, which is capable of imaging 500 000 fps, on loan from the EPSRC loan pool) together with a special mono zoom or a range of Nikon F mount lens together with a General Electric light source.

F. Flow cytometry

In these investigations we ascertained cell viability by a well established population-based bioanalytical approach, namely, flow cytometry, which is a fluorescent activated cell sorting (FACS-Scan) technique. Briefly, the FACS-Scan technique and system employed can quantify both general cell death (necrosis) and programmed cell death (apoptosis). In apoptotic cells, the membrane phospholipids phosphatidylserine (PS) is translocated from the inner to the outer layers of the plasma membrane. During the initial stages of apoptosis, the cell membrane remains intact, while at the time of necrosis the cell membrane loses its integrity and becomes leaky to the vital dye propidium iodide (PI). Staining with annexin V, which has a high affinity for PS in conjunction with PI, allows the identification of living cells (annexin $-PI^-$), early apoptotic cells (annexin $+PI^-$), necrotic cells (annexin $+PI^+$), and debris (annexin $-PI^+$) to give a sensitive measurement of the dynamics of cell death. Several single cell suspensions were prepared from each of the cell samples. Cells were mixed with annexin V fluorescein isothiocyanate (FITC) (final concentration of $1 \mu\text{g ml}^{-1}$) (Pharmlingen, United Kingdom) and PI (final concentration of $1 \mu\text{g ml}^{-1}$) (Sigma, United Kingdom) in the presence of 1.8 mM calcium. Cells were incubated at room temperature for 15 min prior to quenching in calcium containing binding buffer (Pharmlingen, United Kingdom) and were analyzed immediately. A Dako Cytomation CyAn ADP flow cytometer was used to collect data for $>20\,000$ events. The excitation was set at 488 nm using an argon laser; the FITC emission was collected with a 525 ± 20 nm and PI with a 675 ± 20 nm band pass filter. Data were analyzed using SUMMIT 4.3 software (DakoCytomation, United Kingdom). Thus, in these studies the controls and treated cells were passed through the flow cytometry apparatus to analyze the number of living and dead cells through to cells, which were undergoing programmed cell death. Flow cytometry analysis was carried out on three cellular samples, namely, culture controls (CCs) (the cells prepared as a suspension), needle controls (NCs) (which were passed through the device without an applied pressure), and finally, treated samples. Using the above flow cytometry approach, these three samples were analyzed at 0, 7, and 21 days post-treatment. In addition we also analyzed fresh cellular aliquots of the three samples at shorter time points of 24, 48, and 72 h. Repeated flow cytometry analysis was carried out on several fresh samples for both controls and treated samples.

III. RESULTS AND DISCUSSION

While exploring the listed polymers in their many concentrations, these studies traversed a wide operation parametric space for both the applied pressure (0–6 bars) and flow rate ($\sim 10^{-20}$ – 10^{-6} $\text{m}^3 \text{s}^{-1}$) to the pressure chamber and needle(s), respectively. These studies not only assessed the exploration of a single needle device [Figs. 1(a) and 1(b)] but extended to the study of a coaxial needle system [Figs. 1(c) and 1(d)]. Studies were initiated with the exploration of a polyethylene oxide (PEO) solution made into a free-running near-homogeneous polymer solution with added solvents of filtered water and analytical grade ethanol (VWR, Leicestershire, United Kingdom). The prepared solution was syringed into the single needle device at the lowest possible flow rate allowed by our present syringe pump, $\sim 10^{-20}$ $\text{m}^3 \text{s}^{-1}$ (PHD4400, Harvard Apparatus Ltd., Kent, United Kingdom). Once the polymer was seen to reach the exit of the single needle device, a pressure was applied to the chamber, which provided the pressurized by-pass flow through the exit orifices [Fig. 1(b)] placed around the needle exit, which promoted the elongation or drawing of the polymer from the needle exit. At very low flow rates ($\sim 10^{-12}$ $\text{m}^3 \text{s}^{-1}$) for a pressure of ~ 1 bar, the polymer was seen to undergo an unstable threading process [Fig. 2(a)], which was characteristically seen to spin randomly long fiber fragments simultaneously with polymer clusters onto a collecting substrate. The deposited residues at these operational conditions observed under scanning electron microscopy (field emission, JOEL JSM 6301F) revealed a mixture of semisolid to randomly solid coalesced bulk and fiber residues [Fig. 3(a)], respectively. Hence, the flow rate was altered accordingly in conjunction with the applied pressure till stable and continuous fiber spinning was achieved. During this stage a wide operational window was traversed, providing the required experience for understanding the basics of this fiber spinning process, which was observed in real time by way of the high-speed camera. Spinning the PEO solution at an applied pressure to flow rate of ~ 5 bars and $\sim 10^{-11}$ $\text{m}^3 \text{s}^{-1}$, respectively, was seen to generate nanoscaled fibers having a residue range spanning from ~ 35 to ~ 387 nm. The fibers were seen to be near uniform throughout their length. Residue characterization by way of image analysis demonstrated a mean fiber diameter of ~ 215 nm for these operational parameters. We also noticed that elevating the pressure further was seen to form finer fiber residues in the nano-scale.

Although spinning PEO solutions at varied concentrations within a large operational window generated operational parametric clues, it was decided to initiate the introduction of materials into the fibers as this is most relevant to materials sciences and engineering. Thus, several new PEO solutions were formulated with the addition of materials (either nanoparticles and/or nanotubes) at a wide range and concentrations for generating several PEO-based nanosuspensions. Spinning investigations of these nanosuspensions were carried out as previously with the PEO solutions. These studies enabled the understanding of how to manipulate the process as required for forming multicomponent structures.

At an applied pressure to flow rate of ~ 2 bars and $\sim 10^{-10}$ $\text{m}^3 \text{s}^{-1}$ for a PEO nanosuspension containing a nanoparticulate loading of ~ 20 wt %, stable spinning was initiated. High-speed imaging [Fig. 2(b)] and residue analysis [Fig. 3(b)] at these operational parametric conditions revealed the spinning process to form continuous composite fibers in the micrometer range (~ 1 – 5 μm). It was observed that for this PEO-based nanosuspension for a flow rate of $\sim 10^{-10}$ $\text{m}^3 \text{s}^{-1}$ and for an applied pressure of ~ 2 bars, stable and continuous fiber formation was achieved, which was not the case for other nanosuspensions having either different PEO and/or nanomaterial concentrations. Moreover, if the collection time was increased during stable spinning fibers, scaffolds, and multilayered membranes were generated. Maintaining the flow rate of $\sim 10^{-10}$ $\text{m}^3 \text{s}^{-1}$ of the nanosuspension to the single needle device, it was decided to systematically increase the applied pressure to ~ 2.5 , ~ 3 , ~ 3.5 , ~ 4 , ~ 4.5 , and finally ~ 5 bar, while the spinning process was continuously being monitored via the high-speed camera. At these varied applied pressures the generated residues were both collected and analyzed by way of scanning and transmission electron microscopy to assess both their fiber uniformity to any affects the pressure may have on the fiber formation process. At ~ 2.5 bar the spinning process was very similar to that depicted previously for ~ 2 bar [Fig. 2(b)] and did not show any significant effects in fiber

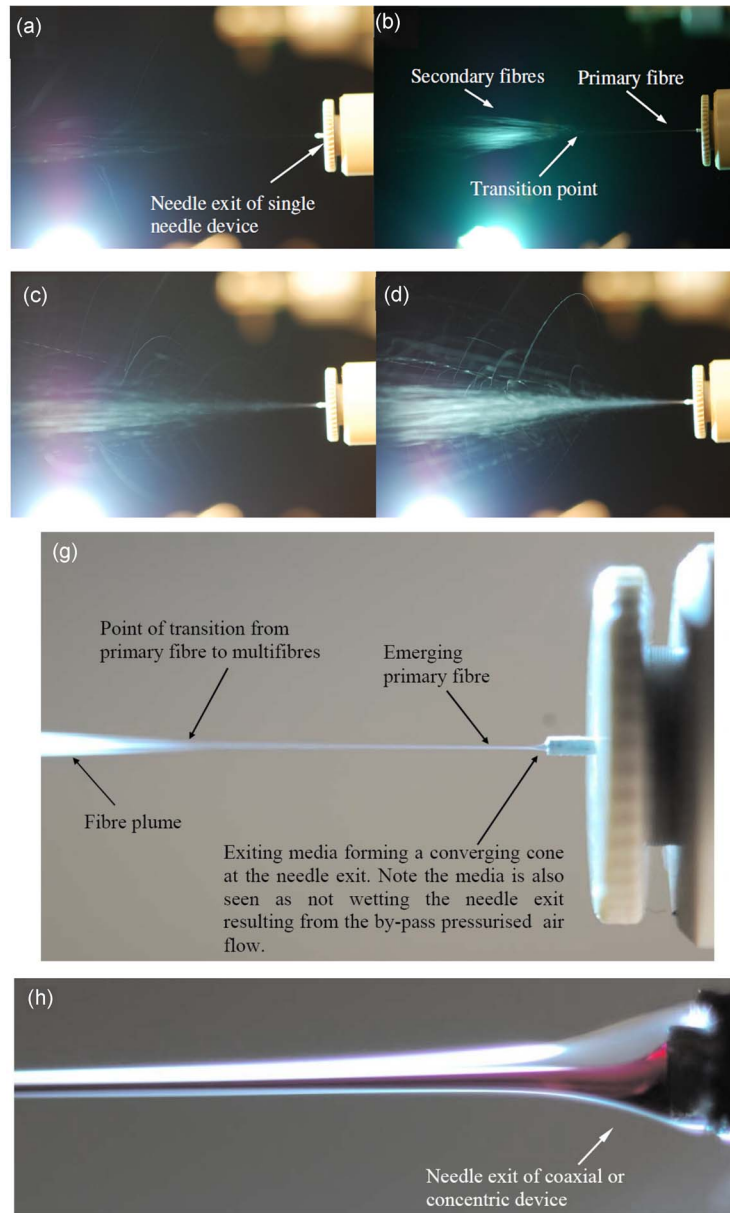


FIG. 2. Representative high-speed digital images of the spinning process in action in the single needle device (a) in the unstable condition and stable spinning conditions at applied pressures of (b) ~ 2 , (c) ~ 3 , (d) ~ 4 , and (e) ~ 5 bar, respectively, for a flow rate of $\sim 10^{-10} \text{ m}^3 \text{ s}^{-1}$. Panel (f) depicts the spinning process in the stable state while varying the flow rate to $\sim 10^{-7} \text{ m}^3 \text{ s}^{-1}$ for a constant applied pressure of ~ 3 bar. Panel (g) depicts the media behavior at the exit of the needle, illustrating the convergence of media together with the nonwetting of the needle. Panel (h) demonstrates the coaxial or concentric needle device at an arbitrary stable operational condition while processing two immiscible nanomaterial-containing suspensions.

distributions. At an applied pressure of ~ 3 bar, we observed that the spinning process was seen to diverge fibers at the needle exit with the forming of multiple fibers [Fig. 2(c)]. The collected residues on analysis showed a significant reduction in the generated fiber diameters, which ranged from $\sim 525 \text{ nm}$ – $3 \text{ }\mu\text{m}$ [Fig. 3(c)]. Similar to the observations made at the applied pressure of ~ 2.5 bar with respect to ~ 2 bar, no significant changes were noted in either the spinning process or the generated fiber distributions at the applied pressure of ~ 3.5 bar with reference to ~ 3 bar. However, on further increasing the applied pressure to ~ 4 bar, we noticed that the spinning

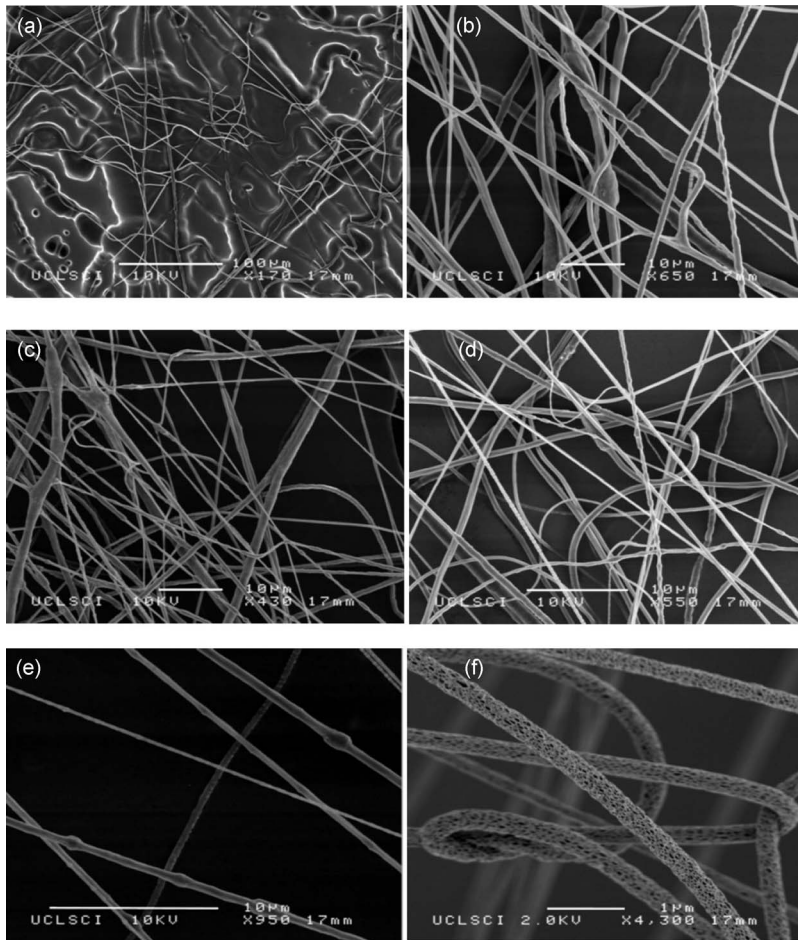


FIG. 3. Characteristic high-resolution scanning electron micrographs illustrating residues collected in (a) the unstable condition and [(b)–(e)] in stable conditions at applied pressures of ~ 2 , ~ 3 , ~ 4 , and ~ 5 bar for a flow rate of $\sim 10^{-10}$ $\text{m}^3 \text{s}^{-1}$ generated by way of the single needle device. Panel (f) depicts a PLLA suspension spun forming a multicomponent porous and fibrous structure at an applied pressure and flow rate of ~ 3 bar and $\sim 10^{-11}$ $\text{m}^3 \text{s}^{-1}$, respectively.

process was seen to further diverge and generate fibers at the needle exit [Fig. 2(d)] and have a notable change in fiber uniformity and distribution [Fig. 3(d)]. At these operational conditions, fibers were seen to be near-uniform throughout their length and were seen to move further toward the nanoscale, hence ranging from ~ 410 nm– 2.5 μm . Elevating the applied pressure to ~ 4.5 bars resulted with the spinning process behaving very similar to that depicted in Fig. 2(d). However, further elevating the applied pressure to ~ 5 bar was seen to generate fibers with a greater divergence at the needle exit [Fig. 2(e)] together with the further reduction in the generated fiber residue distributions. Hence, residues analysis demonstrated a fiber distribution of ~ 25 – 600 nm [Fig. 3(e) and Table I]. Several other PEO solutions and suspensions (containing a wide range of nanomaterials at varied concentrations) were also found to form fibers in stable and continuous states, however, at different operational parametric conditions.

Hence, indicating liquid properties and the introduction of material (concentrations) play a critical role in this fiber spinning approach. Interestingly, we also noted that for any given PEO concentration within a solution, if either the nanoparticle or nanotube loading was increased, this resulted in an overall increase in fiber diameter; this was also the case if the latter was maintained, while the polymer concentration was increased. We believe that this behavior is a direct result of increasing suspension rheological properties or resistance to flow. Our observations via high-speed

TABLE I. Overall fiber characteristics generated by way of pressure driven spinning for a given suspension at a constant applied pressure and flow rate. These characteristics widely vary for the given polymer, added material concentration to the operational parameters, and device setups.

Fiber composition	Applied pressure (bar) ^a	Flow rate (m ³ s ⁻¹) ^b	Distribution	Mean
PEO-only fibers	~5	~10 ⁻¹⁰	~35–387 nm	~215 nm
PEO+20 wt % SiO ₂ nanoparticles	~5	~10 ⁻¹⁰	~25–600 nm	~295 nm
PEO+20 wt % multiwalled bamboo-type nanotubes	~5	~10 ⁻¹⁰	~300 nm–3 μm	~1.7 μm

^aThe applied pressure has an operational accuracy of ± 0.01 bar.

^bFlow rate calibration was carried out before each experiment and was found to have an insignificant variation; however the supply of very high viscosity suspensions had a time delay of ~ 30 s before the selected flow rate was the actual flow rate of that material delivered to the device.

imaging of the spinning process with increasing applied pressure for a constant flow rate showed the point of fiber divergence or transition from primary fiber to multifibers varied with the applied pressure; hence this point moved closer to the needle exit with the increasing applied pressure. We envisage that this behavior is directly due to the generated pressurized by-pass three-dimensional conical air plumes expanding on leaving the exit orifices with the increasing applied pressure.

Contrary to maintaining the flow rate for an increasing applied pressure, if the reverse took (constant applied pressure of ~ 3 bars for an increasing flow rate to $\sim 10^{-7}$ m³ s⁻¹) place, high-speed imaging would illustrate the fiber spinning process, demonstrating a higher density of generated fibers emerging the needle exit, which is not surprising; however we additionally noticed the fiber plume converging [Fig. 2(f)] with the increase in flow rate. Furthermore, the increase in flow rate also gave rise to the multifiber generation point to move further away from the needle exit with increasing flow rate. At this time we speculate plume convergence taking place due to the increase in the density of outflowing material from the needle. This was not the case while the out flow was maintained for a rising applied pressure, and hence we hypothesize that this is due to the pressurized by-pass flow having a more pronounced effect on the lower density of exiting material being susceptible to the interfering by-pass or cross flowing pressure flow dynamics exiting the six orifices [Fig. 1(b)]. The increase in material outflow had a similar effect as increasing the media viscosity, namely, increasing the overall fiber diameter. We also noted that during these studies, pressure driven spinning converged the exiting media at the needle exit, which assisted in forming fine micro/nanometer scaled fibers for a given flow rate to applied pressure for a device setup [Fig. 2(g)].

Fibers generated by spinning these PEO-based nanosuspensions on analysis by way of both energy-dispersive x rays [Figs. 4(a) and 4(b)] and selected area diffraction [Fig. 4(c)] identified the addition of SiO₂ nanoparticles, which are amorphous in nature. Similarly, high-resolution transmission electron microscopy revealed the embedded nanotubes within the polymeric nanosuspensions [Figs. 4(d)–4(f)] containing 20 wt % of nanotubes. Figure 4(f) depicts the diffraction pattern demonstrating the nanocrystalline properties of these explored nanotubes. Increasing the spinning and collection of either nanosuspension over a longer time span was seen to generate composite multilayered scaffolds and membranes [Fig. 4(g)]. Characteristically similar structural entities were generated by means of other polymer blends with nanomaterials. During fiber characterization, we noticed that for the same PEO concentration in those respective nanosuspensions (containing either 20 wt % of nanoparticles or nanotubes), the resulting residues were larger for the nanotube-based suspensions in comparison to those containing nanoparticulates (Table II). We note that this is directly due to the nanotube dimensions, which are ~ 10 – 15 nm in diameter but lengthwise varied from ~ 1 – 5 μm, hence generating larger residues. In these studies, we also prepared several poly(L-Lactic acid) (PLLA) (Mw=700 000, Polysciences, Inc., Warrington, USA) based suspensions (1–5 wt %), which were dissolved in dichloromethane (DCM), with and without the addition of nanomaterials at concentrations ranging from 1 to 20 wt %. Our reason for exploring this polymer (PLLA) dissolved in DCM is based on previous electrospinning studies,

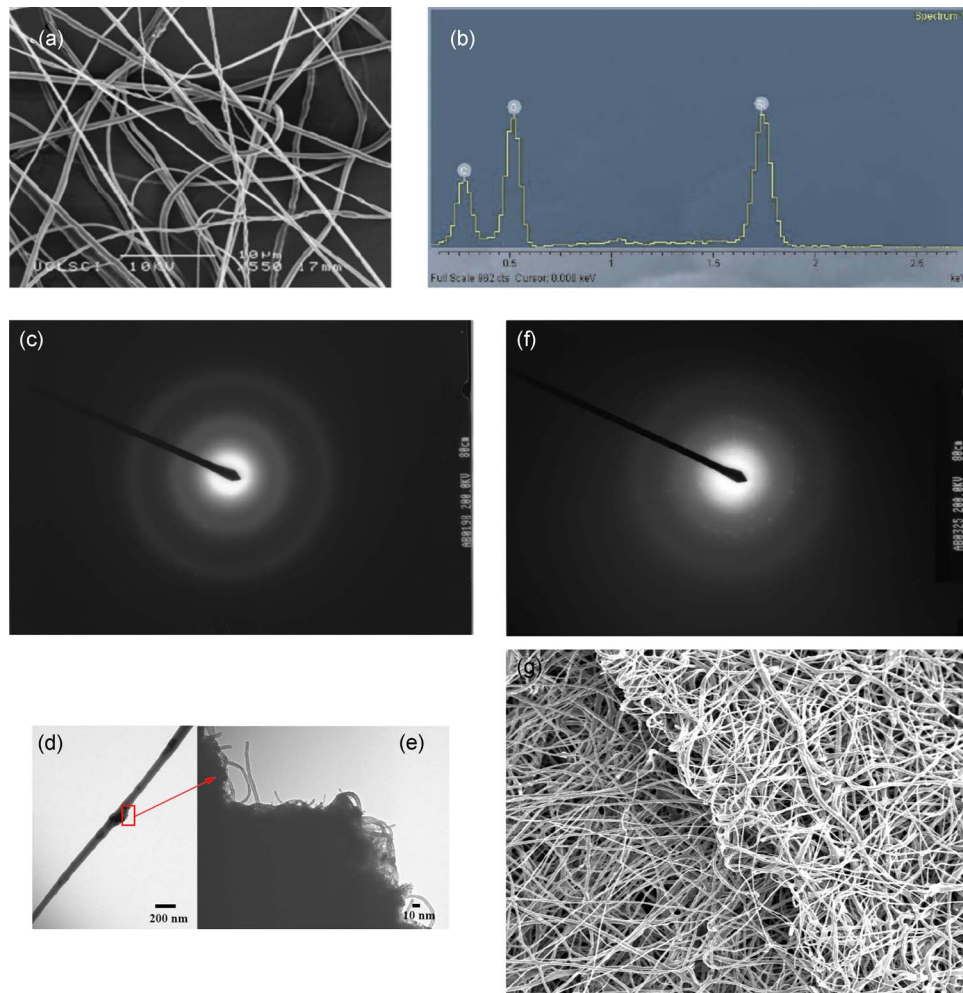


FIG. 4. Panels (a) and (b) demonstrate an electron micrograph of the composite fibers and materials analysis carried out using energy-dispersive x rays, which illustrate the existence of SiO₂ nanoparticulates within the fibers. Panel (c) depicts the diffraction pattern of those nanoparticulate-bearing fibers demonstrating the amorphous nature of these SiO₂ nanoparticulates. Transmission electron micrographs (d) and (e) depict characteristic fibers that contain bamboo-type multiwalled nanotubes, which were added into the polymer solution during its formulation. Panel (f) illustrates the nanocrystalline properties of these embedded nanotubes. Finally, the scanning electron micrograph (g) represents a multicomponent and multilayered scaffold/membrane generated by way of collecting the generated fibers via a single needle device over a long time span (~ 1200 s).

which demonstrated this fast evaporating solvent forming porous fibers during the spinning process.¹⁶ The PLLA-alone suspension spun at stable conditions (applied pressure and flow rate of ~ 2.5 bars and $\sim 10^{-11}$ m³ s⁻¹, respectively) and were found to directly generate multicompositional porous structural residues [Fig. 3(f)], much like those generated in electrospinning investigations. The operational conditions required modification of handling those PLLA nanosuspensions, which were also seen to generate multicomponent entities having a porous surface morphology.

Comparable to those investigations carried out with the single needle device, we initiated our studies with the concentric or coaxial needle device, as we wanted to probe the versatility of this approach for processing two immiscible suspensions. Techniques possessing the ability to handle two immiscible media for forming multistructured or co-structured and composite entities have widespread applications spanning biology and medical areas of research and development. Hence, these studies were initiated with PEO and poly(ϵ -caprolactone) (PCL) solutions, which were

TABLE II. Population-based cell viability assessment by way of flow cytometry showing the cellular dynamics of those treated in comparison to the controls. The cell populations tabulated were near identical for those primary and mesenchymal stem cells handed by way of this spinning process.

Cellular dynamics	Culture control (CC) ^a			Needle controls (NCs) ^b			Pressure driven samples ^c		
Apoptotic	0.18	4.95	0.21	0.53	3.21	0.19	0.21	3.31	0.17
Live	97.85	78.11	70.34	96.71	81.37	71.58	97.31	80.76	73.41
Necrotic	0.06	11.32	4.82	0.05	10.14	5.68	0.03	9.85	5.34
Cell debris	1.91	5.62	24.63	2.71	5.28	22.55	2.45	6.08	21.08
Days	0	7	21	0	7	21	0	7	21

^aThese are those cells that have not been treated to any form of spinning, etc.

^bThese cells are those that have been put through the device without the application of the driving mechanism.

^cCells that have undergone pressure driving spinning. The data in Table II are representative of three individual experiments.

prepared into free flowing solutions with water and ethanol and acetone, respectively. However, in the present context we also explored a second media that flowed in the inner needle, which initially we varied from pressurized air to aqueous eosin Y, or 8-hydroxypyrene-1,3,6-trisulfonic acid trisodium salt (solvent green 7) mixed with and without a wide range of miscible media. The flow rates for both the inner and outer media could be consistently varied from $\sim 10^{-20}$ – 10^{-6} $\text{m}^3 \text{s}^{-1}$ with the variation in the syringe in combination with the syringe pump flow control. Preliminary studies were carried out by setting the flow rates of both the inner and outer needles to the lowest possible flow rate ($\sim 10^{-20}$ $\text{m}^3 \text{s}^{-1}$). Subsequently, on seeing the media exiting the coaxial needle system, a pressure was applied and visualized with the aid the high-speed camera. Unlike in the single needle fiber generation process, we avoided the splitting of the primary fiber to multiple fibers by diffusing the direct pressurized by-pass flow to well above the needle exits. This ensured the formation of co-structured fibers. A wide range of flow combinations for the inner and outer flow rates to applied pressures was investigated (from 0–6 bar and $\sim 10^{-20}$ – 10^{-6} $\text{m}^3 \text{s}^{-1}$ for the applied pressure and flow rate, respectively). Additionally, spinning stability was confirmed both visually [Fig. 2(f)] and by way of residue analysis. Much like in the single needle spinning scenario media, properties together with concentrations of either the polymer or nanomaterial were seen to have effects on the generation of composite fibers in this needle arrangement [Figs. 1(c) and 1(d)]. Several costructures were fabricated, having near-uniformity along the length of the fiber residue. Operational parametric studies for the coaxial needle system showed that the flow rate of media accommodated within the outer needle had to have a flow rate larger than that of the inner needle for complete and consistent encapsulation of the inner media. Thus, a PCL solution at a concentration of ~ 5 wt % flowing at $\sim 10^{-8}$ $\text{m}^3 \text{s}^{-1}$ with the aqueous eosin Y or 8-hydroxypyrene-1,3,6-trisulfonic acid trisodium salt (solvent green 7) flowing at $\sim 10^{-9}$ $\text{m}^3 \text{s}^{-1}$ was seen to form costructures, which demonstrated fiber uniformity as residues [Fig. 5(a)]. We also found that air or media having no elongational characteristics (low viscosity < 300 mPa s) flowing within the inner needle could be encapsulated by a high viscosity fluid flowing within the outer needle for forming fibers containing beaded inner structures [Fig. 5(b)].

If the introduction of air to the inner needle was increased, a point was reached where continuous hollow fibers were found to form. Thus combining this feature with the multi-PLLA suspension spun in the single needle scenario, it was possible to generate composite multistructural fibers, which were both hollow and porous [Figs. 5(c)–5(e)]. During the fabrication of these multistructural fibers, we found that there are several critical parameters, which depend on media composition, and operational parameters for the device setup that have a significant influence on the formation of such structures. Additionally, the driving pressure exiting the device exit orifices, explored for drawing out these fibers, was also seen as having an effect on the exterior morphology of these structures. This was observed while varying the driving pressurized air flow from ~ 3 to ~ 5 bars, which showed the effects on the pores on the surface of the fibers varying from

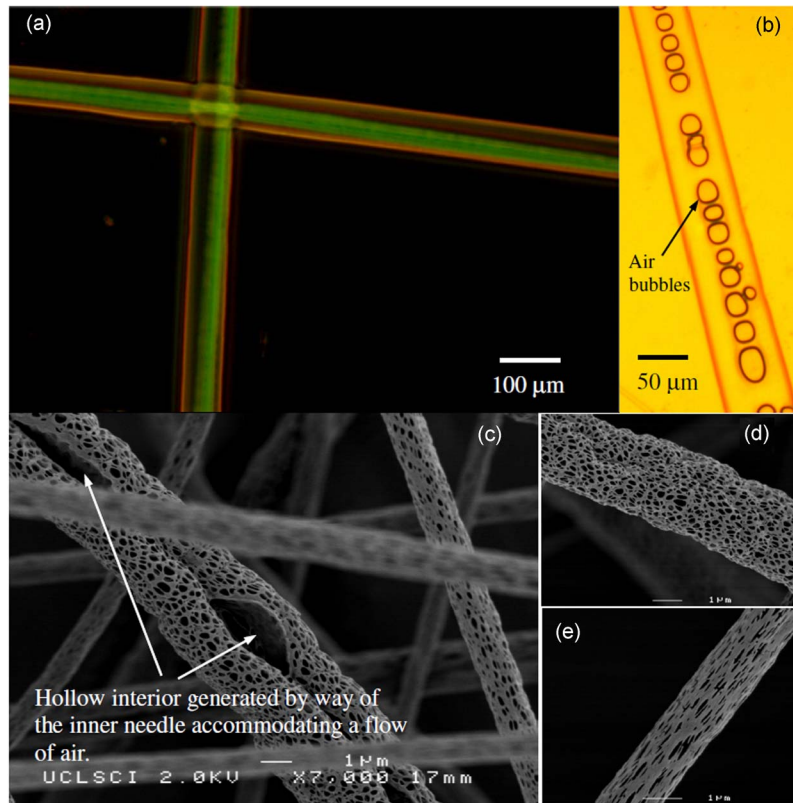


FIG. 5. Illustrative micrographs (a) fluorescence in combination with optical and (b) optical alone demonstrating the multicompositional structures that could be fabricated with the coaxial pressure driven device. (c) demonstrates a typical hollow and porous fibrous structure imaged via high-resolution scanning electron microscopy while processing a PLLA based concentrated nanosuspension. Panels (d) and (e) illustrate the effect of driving pressure on the morphology in surface porosity.

near-spherical-like porous [Fig. 5(d)] to those that were near-oblong [Fig. 5(e)] in morphology. This characteristic was also observed in the single needle spinning of PLLA suspensions. We also observed that while elevating the inner air flow past an upper critical point for a given suspension, generating fibers were seen to split open, resulting in structural morphologies resembling porous leaves.

On developing this spinning approach, it was endeavored to apply this direct fiber spinning approach across the three materials boundaries, namely, structural, functional, and biological. Thus, we explored the ability to directly form fibers nesting living cells. For these investigations, we explored aqueous polyvinyl alcohol (PVA)-alone to those PVA blends, which contained water and/or phosphate buffer saline based PEO suspensions. The cells investigated in these studies were an immortalized T293 cell line. The respective cells were mixed with the aqueous PVA solution at $\sim 1:10$ and spun in a laminar flow safety hood. Figure 6(a) depicts the generated living scaffold containing those respective cells. The choice in exploring PVA and/or PEO solutions for cell encapsulation was based on the ability of retaining the cells post-treatment, as these polymers dissolve in cell friendly media, which subsequently were assessed as populations for their viability. Therefore, in these studies we interrogated cellular viability by way of cell labeling in conjunction with flow cytometry. Cells were assessed at three time points post-treatment in comparison to controls and were seen to be indistinguishable (Table II). The controls referred in this context are those that have been passed through the device without the driving mechanism (referred to as the NC) and those CCs, which are those cells that have not been subjected to any form of treatment. During these studies, we noted that the needle diameter and the rate of cell suspen-

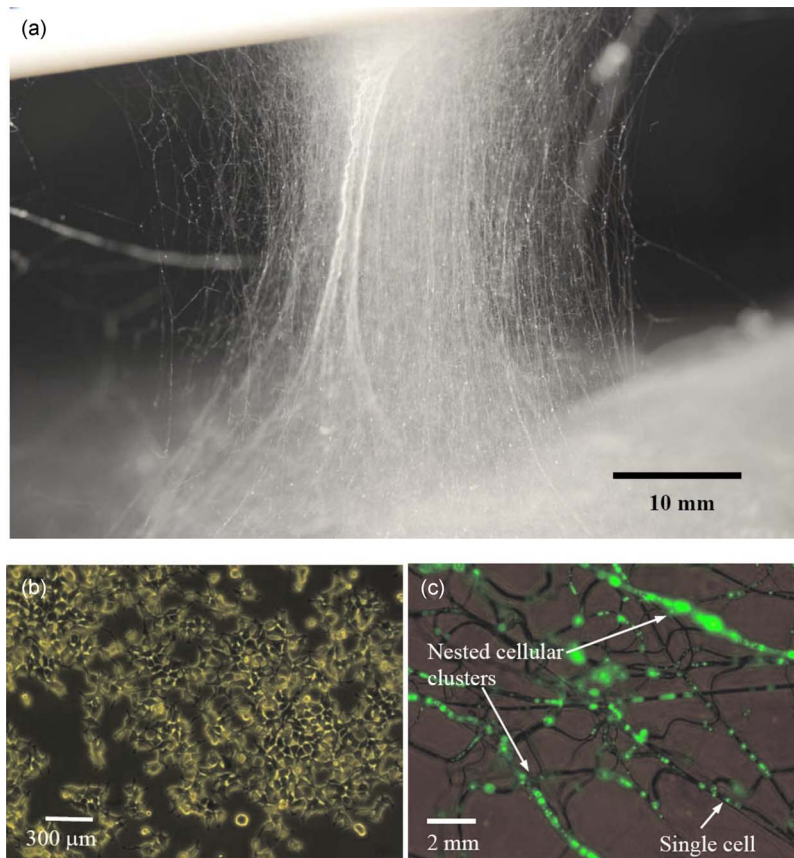


FIG. 6. Typical (a) digital image of a cell-bearing living scaffold/membrane, (b) post-treated near-confluent cells, which were indistinguishable with those controls, and (c) fluorescent and optical image depicting the scaffold nesting living cells.

sion being syringed through the needle have an effect on cell viability. However, this was overcome with ease with the increase in needle bore diameter, which eliminated this effect. The increase in needle bore diameter also had no effect on the generated residues. This is due to this process sharing the effect of converging [Fig. 2(g)] the exiting media at the needle exit by way of the by-pass flowing pressure, which is also a feature exploited by electrospinning but with the aid of a high intensity electric field. In these biological studies, we performed two subset experiments, namely, (a) we investigated cell viability with the aid of flow cytometry and (b) we wished to study cell placement or cell-nesting characteristics of these living entities. The former employed unlabelled cells until required for flow cytometry, while the latter used eGFP-expressing cells with fluorescence microscopy.

For flow cytometry analysis, several cell samples for each sample [CC, NC, and pressure driven spinning (PDS)] having a cell population $>10^6$ cells were labeled with annexin V (Invitrogen Ltd., Paisley, United Kingdom) together with PI and analyzed. Cytometry data demonstrated that the treated samples were indistinguishable from the controls over the three time points (Table II). This was also the case if we assessed cellular viability at time points 24, 48, and 72 h post-treatments. In addition to these cell viability investigations, our phenotypic studies demonstrated that cell confluence was reached by the three samples at nearly the same time [Fig. 6(b)]. As previously mentioned, we also wanted to assess cell-nesting characteristics of these cells within the generated cell-bearing fibers; for these studies we labeled cells with a lentivirus eGFP construct as previously described.^{19,20} Thus, analysis of these spun and collected samples demonstrated cellular clustering of cells within the fibers [Fig. 6(c)]. Interestingly, the cellular viabilities

reported in these studies are comparable to those cell electrospinning studies,^{13,14} thus demonstrating the ability to compete in this arena with the additional advantage of not possessing the hazardous high-applied voltage.

IV. CONCLUSIONS

Our developmental studies on pressure driven spinning has unveiled a direct fiber spinning process comparable to electrospinning, with the advantages of both the removal of the high intensity electric field and the possibility of exploring this approach for handling highly conducting suspensions (containing sensitive molecules) in the single needle configuration. Moreover, these investigations have shown the ability to explore this approach for the direct fabrication of composite fibers, scaffolds, and membranes to those having porous textured surfaces. The process has been applied for the direct handling of structural, functional, and biological materials, which demonstrate the versatility of this approach having applicability in the biomedical sciences. In a materials sciences and engineering standpoint, the authors are vigorously pursuing investigations on what parameters have an effect on the controlled fabrication of wall thickness when generating size-controlled fibers, scaffolds, and membranes. In parallel we are in the process of optimizing the spinning approach, for example, encapsulating single cells placed uniformly along the fiber, which is most important if this protocol is to endeavor as a cell therapeutic approach to the ability of forming controlled fibers, scaffold, and membranes, which will assist in forming three-dimensional preorganized cell cultures. The post-treated cells are also currently in the process of being assessed at a genetic, genomic, and physiological level by means of gene chip microarrays and reverse transcription polymerase chain reaction to cytogenetic studies, which will further assess the process as a potential direct cell handling approach. Thus, the authors' intentions are to completely assess this fiber spinning protocol, so this technology may compete head-to-head with its rival, electrospinning in the fiber to scaffold and membrane preparation arena.

ACKNOWLEDGMENTS

S.N.J. wishes to specially thank Dr. Carl Lance and Dr. David Catone of Nyacol Nano Technologies, Inc., Dr. David Carnahan, President of NanoLab, Inc., for the in-kind supply of nanoparticles and nanotubes, respectively, which have been extensively explored in these investigations.

- ¹J. B. Fenn, M. Mann, C. K. Meng, S. F. Wong, and C. M. Whitehouse, *Science* **246**, 64 (1989).
- ²S. N. Jayasinghe, *Regenerative Medicine* **3**, 49 (2008).
- ³G. I. Taylor, *Proc. R. Soc. London, Ser. A* **280**, 383 (1964).
- ⁴L. Larrondo and R. St. Manley, *J. Polym. Sci., Part A-2* **19**, 909 (1981).
- ⁵K. McQuinn, F. Hof, and J. S. McIndoe, *Int. J. Mass Spectrom.* **279**, 32 (2009).
- ⁶S. N. Jayasinghe, *Biomedical Materials* **3**, 034004 (2008).
- ⁷A. C. Sullivan, K. Scott, and S. N. Jayasinghe, *Macromol. Chem. Phys.* **208**, 2032 (2007).
- ⁸A. C. Sullivan and S. N. Jayasinghe, *Biomicrofluidics* **1**, 034103 (2007).
- ⁹S. N. Jayasinghe and A. C. Sullivan, *J. Phys. Chem. B* **110**, 2522 (2006).
- ¹⁰S. N. Jayasinghe, A. N. Qureshi, and P. A. M. Eagles, *Small* **2**, 216 (2006).
- ¹¹A. Abeyewickreme, A. Kwok, J. R. McEwan, and S. N. Jayasinghe, *Integrated Biology* **1**, 260 (2009).
- ¹²P. Joly, B. Jennings, and S. N. Jayasinghe, *Biomicrofluidics* **3**, 044107 (2009).
- ¹³A. Townsend-Nicholson and S. N. Jayasinghe, *Biomacromolecules* **7**, 3364 (2006).
- ¹⁴S. N. Jayasinghe, S. Irvine, and J. R. McEwan, *Nanomedicine* **2**, 555 (2007).
- ¹⁵M. Bognitzki, T. Frese, M. Steinhart, A. Greiner, and J. H. Wendorff, *Polym. Eng. Sci.* **41**, 982 (2001).
- ¹⁶D. Li and Y. Xia, *Adv. Mater. (Weinheim, Ger.)* **16**, 1151 (2004).
- ¹⁷A. Greiner and J. H. Wendorff, *Angew. Chem., Int. Ed.* **46**, 5670 (2007).
- ¹⁸Y. Srivastava, M. Marquez, and T. Thorsen, *Biomicrofluidics* **3**, 012801 (2009).
- ¹⁹A. Kwok, S. Arumuganathar, S. Irvine, J. R. McEwan, and S. N. Jayasinghe, *Biomedical Materials* **3**, 025008 (2008).
- ²⁰E. Ward, E. Chan, K. Gustafsson, and S. N. Jayasinghe, "Combining bio-electrospraying with gene therapy: A novel biotechnique for the delivery of genetic material via living cells," *Analyst*, DOI: 10.1039/b923307e.